CHEMISTRY
A EUROPEAN JOURNAL

DOI: 10.1002/chem.200701487

A Family of Enneanuclear Iron(II) Single-Molecule Magnets

Athanassios K. Boudalis,*[a] Yiannis Sanakis,*[a] Juan Modesto Clemente-Juan,[b] Bruno Donnadieu,[c] Vassilios Nastopoulos,[d] Alain Mari,[e] Yanick Coppel,[e] Jean-Pierre Tuchagues,[e] and Spyros P. Perlepes[d]

Abstract: Complexes $[Fe_9(X)_2(O_2CMe)_8\{(2\text{-py})_2CO_2\}_4]$ ($X^- = OH^-$ (**1**), N_3^- (**2**), and NCO^- (**3**)) have been prepared by a route previously employed for the synthesis of analogous Co_9 and Ni_9 complexes, involving hydroxide substitution by pseudohalides (N_3^-, NCO^-). As indicated by DC magnetic susceptibility measurements, this substitution induced higher ferromagnetic couplings in complexes **2** and **3**, leading to higher ground spin states compared to that of **1**. Variable-field experiments have shown that the ground state is not well isolated from excited states, as a result of which it cannot be unambiguously determined. AC susceptometry has revealed out-of-phase signals, which suggests that these complexes exhibit a slow relaxation of magnetization that follows Arrhenius behavior, as observed in single-molecule magnets, with energy barriers of 41 K for **2** ($\tau_0 = 3.4 \times 10^{-12}$ s) and 44 K for **3** ($\tau_0 = 2.0 \times 10^{-11}$ s). Slow magnetic relaxation has also been observed by zero-field ^{57}Fe Mössbauer spectroscopy. Characteristic integer-spin electron paramagnetic resonance (EPR) signals have been observed at X-band for **1**, whereas **2** and **3** were found to be EPR-silent at this frequency. ^{1}H NMR spectrometry in CD_3CN has shown that complexes **1**–**3** are stable in solution.

Keywords: iron · magnetic properties · Moessbauer spectroscopy · polynuclear iron(II) complexes · single-molecule magnets

Introduction

Considerable attention has been devoted to single-molecule magnets (SMMs) in recent years.[1] These molecules exhibit slow relaxation of their magnetization at low temperatures, which, though of a different physical origin, is phenomenologically reminiscent of that encountered in classical bulk magnets and superparamagnetic nanoparticles. The most striking characteristics of these materials are their molecular nature and their small and homogeneous sizes, which are in sharp contrast to classical magnets and magnetic nanoparticles. These properties have led researchers to propose applications of high technological interest for these molecules, such as use in high-density magnetic storage media.[2] The observation of quantum tunneling of their magnetization (QTM)[3] has also led to the proposal that SMMs might be exploited as quantum bits (qubits) in quantum computing.[4] Recently, the proposal to use SMMs in diagnostic imaging (e.g., as enhanced MRI contrasting agents) has been examined.[5] Beyond this, SMMs may potentially address problems concerning size homogeneity and, by virtue of their facile chemical modification, may provide solutions for issues of solubility, drug delivery, cellular recognition, and toxicity.

[a] Dr. A. K. Boudalis, Dr. Y. Sanakis
Institute of Materials Science, NCSR "Demokritos"
15310 Aghia Paraskevi Attikis (Greece)
Fax: (+30) 210-6519430
E-mail: tbou@ims.demokritos.gr

[b] Dr. J. M. Clemente-Juan
Instituto de Ciencia Molecular, Universidad de Valencia
c/Doctor Moliner, 50, 46100 Burjassot (Spain)

[c] B. Donnadieu
Department of Chemistry,
University of California at Riverside
Riverside, CA 92521 (USA)

[d] Prof. V. Nastopoulos, Prof. S. P. Perlepes
Department of Chemistry, University of Patras
26504 Patras (Greece)

[e] Dr. A. Mari, Dr. Y. Coppel, Prof. J.-P. Tuchagues
Laboratoire de Chimie de Coordination du CNRS, UPR 8241
205 route de Narbonne, 31077 Toulouse Cedex 04 (France)

Supporting information for this article is available on the WWW under http://www.chemeurj.org/ or from the author: ORTEP plot of complex **2**; multifield $\chi_M T$ versus T data and fitted low-temperature Mössbauer spectra for complexes **1** and **2**; selected interatomic distances and bond angles for complexes **1**–**3**.

Moreover, besides these potential practical applications, research into single-molecule magnetism has provided the necessary impetus for fundamental research in the area of magnetism and molecular magnetic materials. Following the discovery and initial studies of the SMM phenomenon in relation to the complex $[Mn_{12}O_{12}(O_2CMe)_{16}(H_2O)_4]$,[6] which has since been exhaustively studied, a host of molecules displaying the same property have been synthesized. These include complexes with S values ranging from 2[7] to 83/2[8] and nuclearities ranging from 1[9,10] to 84.[11] These molecules have often exhibited complicated and unexpected behaviors, which have tested, and continue to test, current theoretical models for magnetism.

Iron(II) is ideally suited for the preparation of SMMs, since it combines a large spin ($S=2$) with a significant single-ion magnetic anisotropy. In addition, iron(II) complexes give us the opportunity to probe their electronic structures not only with a set of bulk (susceptometry) or microscopic techniques (EPR, NMR, and inelastic neutron scattering (INS) spectroscopies, etc.), but also with ^{57}Fe Mössbauer spectroscopy, which is a powerful tool for extracting information that is not available through other techniques. Iron(II) exhibits Mössbauer parameters that are very sensitive to the ligand environment, temperature, and magnetic field, and are therefore very valuable for a theoretical interpretation. Finally, we felt that our prior knowledge of the corresponding cobalt(II)[12,13] and nickel(II)[14] chemistry would give us the opportunity to obtain complexes with desired structures and magnetic properties.

Herein, we report the extension of this chemistry to iron(II). In particular, we report for the first time on the structure and magnetic properties of the hydroxo complex $[Fe_9(OH)_2(O_2CMe)_8\{(2\text{-py})_2CO_2\}_4]$ (**1**). Its reactivity towards pseudohalides has led to the previously reported azido complex $[Fe_9(N_3)_2(O_2CMe)_8\{(2\text{-py})_2CO_2\}_4]$ (**2**)[15] and to the new cyanato complex $[Fe_9(NCO)_2(O_2CMe)_8\{(2\text{-py})_2CO_2\}_4]$ (**3**), for which there is no known analogue. Detailed magnetic studies on **1**–**3** have shown that pseudohalide substitution in **1** has a marked effect on the magnetic properties of complexes **2** and **3**, which behave as single-molecule magnets. This family of SMMs represents the second example of an iron(II) SMM family, besides the cubane complexes $[Fe_4(L)_4(MeOH)_4]$ ($L=sae^{2-}$, the dianion of 2-salicylideneamino-1-ethanol,[16] and L = 5-Br-sae or 3,5-Cl_2-sae,[17] the respective bromo and chloro derivatives thereof), while we have recently reported $[Fe_2(NCO)_3(acpypentO)]$ as another Fe^{II} SMM.[18]

Abstract in Greek:

Τα σύμπλοκα $[Fe_9(X)_2(O_2CMe)_8\{(2\text{-py})_2CO_2\}_4]$ (X^- = OH^- (**1**), N_3^- (**2**) και NCO^- (**3**)) παρασκευάστηκαν μέσω μιας συνθετικής πορείας που είχε προηγουμένως χρησιμοποιηθεί για την σύνθεση των αναλόγων συμπλόκων Co_9 και Ni_9, και που περιλαμβάνει αντικατάσταση υδροξειδίων από ψευδαλογονίδια (N_3^-,NCO^-). Όπως έδειξαν οι μετρήσεις μαγνητικής επιδεκτικότητας DC, αυτή η αντικατάσταση επέφερε ισχυρότερες σιδηρομαγνητικές συζεύξεις στα σύμπλοκα **2** και **3** οδηγώντας σε υψηλότερου σπιν βασικές καταστάσεις σε σύγκριση με του **1**. Πειράματα μεταβαλλόμενου πεδίου έδειξαν ότι η βασική κατάσταση δεν είναι καλά διαχωρισμένη από τις διηγερμένες, οπότε δεν μπορεί να προσδιοριστεί σαφώς. Μετρήσεις μαγνητικής επιδεκτικότητας AC αποκάλυψαν σήματα εκτός φάσης που υποδεικνύουν ότι αυτά τα σύμπλοκα παρουσιάζουν βραδεία χαλάρωση της μαγνήτισης που ακολουθεί συμπεριφορά Arrhenius, όπως παρατηρείται στους Μονομοριακούς Μαγνήτες, με ενεργειακά φράγματα 41 K (για το **2**, $\tau_0 = 3.4\times10^{-12}$ s) και 44 K (για το **3**, $\tau_0 = 2.0\times10^{-11}$ s). Βραδεία μαγνητική χαλάρωση επίσης παρατηρήθηκε με φασματοσκοπία ^{57}Fe Mössbauer μηδενικού πεδίου. Σήματα Ηλεκτρονιακού Παραμαγνητικού Συντονισμού (EPR), χαρακτηριστικά ακεραίου σπιν παρατηρήθηκαν στην περιοχή X για το **1**, ενώ τα **2** και **3** δεν έδωσαν σήματα EPR σε αυτήν την συχνότητα. Φασματοσκοπία ^{1}H NMR σε CD_3CN έδειξε ότι τα σύμπλοκα **1**-**3** είναι σταθερά σε διάλυμα.

Results and Discussion

Syntheses: The syntheses of complexes **1**–**3** were based on previously reported syntheses of the Co^{II} and Ni^{II} analogues. The Co_9 clusters were synthesized from MeCN solutions, whereas the Ni_9 clusters were obtained from DMF solutions. It was decided to employ MeCN as the solvent here since it has a lower boiling point than DMF and therefore offered the possibility of obtaining crystals through slow evaporation techniques as well as access to totally desolvated samples.

The synthesis of complex **1** may be summarized by Equation (1):

$$9\,Fe(O_2CMe)_2\cdot 1.75\,H_2O + 4\,(2\text{-py})_2CO \xrightarrow[\Delta]{MeCN} [Fe_9(OH)_2(O_2CMe)_8\{(2\text{-py})_2CO_2\}_4]\ (\mathbf{1}) + 10\,MeCO_2H + 9.75\,H_2O \quad (1)$$

It is noteworthy that the color change of the solution, from dark blue-green to dark red (the color of the complex), occurred only after heating. This indicates that hydration of the $(2\text{-py})_2CO$ ligand and formation of the complex requires a significant activation energy. The same observation was made in relation to the syntheses of the corresponding Co^{II} and Ni^{II} complexes. However, the formation of polynuclear Fe^{III} complexes with the same ligand[19] occurred at ambient temperature, indicating different behavior of the ligand towards divalent and trivalent metal ions.

For complexes **2** and **3**, in addition to the initially established synthetic route via complex **1**, it was also found that they were accessible through in situ reaction of iron(II) acetate, $(2\text{-py})_2CO$, and the respective pseudohalide salt. This route, represented by Equation (2), led straightforwardly to the desired complexes in high yields.

$$9\,Fe(O_2CMe)_2\cdot 1.75\,H_2O + 4\,(2\text{-py})_2CO + 2\,(NaN_3,KOCN) \xrightarrow[\Delta]{MeCN} [Fe_9(N_3,NCO)_2(O_2CMe)_8\{(2\text{-py})_2CO_2\}_4]\ (\mathbf{2},\mathbf{3}) + 8\,MeCO_2H + 2\,(Na,K)O_2CMe + 11.75\,H_2O \quad (2)$$

In addition, it seemed interesting to test whether we could replace the μ_4-OH^- ligand of **1** by a μ_4-NC^- ion. To this end, KCN was used as the pseudohalide salt. However, applying the synthetic procedure used to obtain **2** and **3** led to a dark-red solid identified as **1** through IR spectroscopy and

elemental analysis, reflecting the weaker bridging ability of cyanide as compared to azide and cyanate.[20]

Description of the structures: The structures of complexes **1–3** are strikingly similar (see Figure 1, Figure 2, and Figure S1, and Tables S1–S3 in the Supporting Information), and therefore only that of complex **3** is analyzed here, and moreover, not in great detail due to its similarity to those of the Co^{II} and Ni^{II} complexes.

The complex consists of eight iron(II) ions forming two slightly staggered parallel squares, with a ninth iron(II) ion located between them. Bridging within the squares is achieved through a μ_4-NCO^- ligand, four *syn*,*syn*-μ_2:η^1:η^1-acetato anions, and four alkoxo oxygen atoms of the $(2\text{-py})_2CO$ ligand. The alkoxo oxygen atoms are μ_3, since they also bridge the square bases to the central iron, which is therefore octacoordinated. The $(2\text{-py})_2CO$ ligand is in its usual bis-deprotonated *gem*-diol form, $(2\text{-py})_2CO_2^{2-}$, assuming a μ_5:η^1:η^3:η^3:η^1 coordination mode.

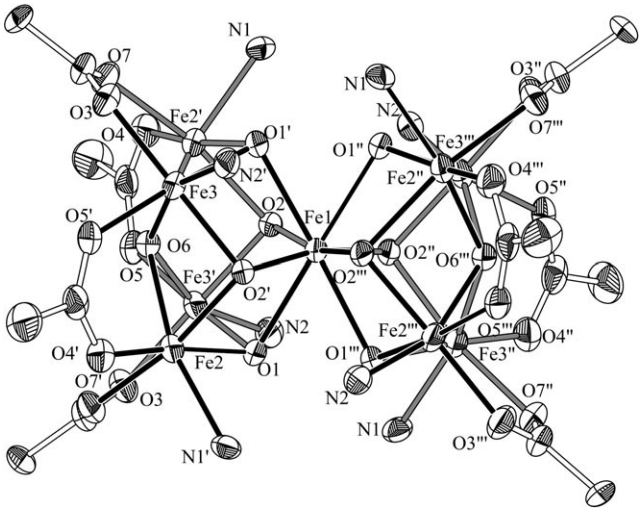

Figure 1. ORTEP plot of complex **1** (thermal ellipsoids set at the 30% probability level). All H atoms and all non-coordinated atoms of the $(2\text{-py})_2CO_2^{2-}$ ligands have been omitted for clarity. See Table S1 in the Supporting Information for detailed bond lengths, angles, and symmetry operation symbols.

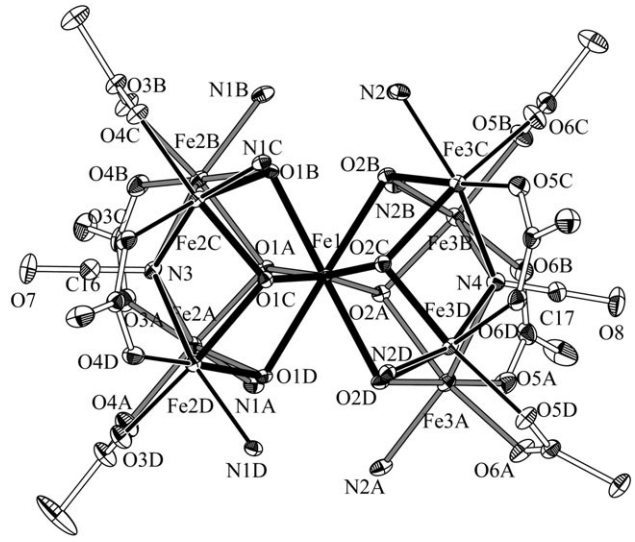

Figure 2. ORTEP plot of one of the two independent molecules of complex **3** (thermal ellipsoids set at the 30% probability level). All H atoms and all non-coordinated atoms of the $(2\text{-py})_2CO_2^{2-}$ ligands have been omitted for clarity. See Table S3 in the Supporting Information for detailed bond lengths and angles.

The μ_4-OH^- bridging mode in **1** is rather rare, having only been observed in a few transition metal[21,22] and lanthanide(III)[23–26] complexes. Two such cases are the enneanuclear complex cations of $[Sm_9(acac)_{16}(OH)_{10}][Cr_2(CO)_{10}(\mu\text{-H})]$[24] and $[Tb_9(Hesa)_{16}(\mu\text{-OH})_{10}](NO_3)$,[25] the metal cores of which, consisting of two square Ln_4 bases flanking a central Ln atom, display striking structural resemblance to those of complexes **1–3**. In these cases, however, the hydroxo oxygen atom presents an almost square geometry; the Sm-O-Sm angles are in the range 167–170° and the Tb-O-Tb angles are 168.9°, and hence the oxygen atom is positioned much closer to the Ln_4 planes. The μ_4 end-on bridging mode is even rarer for the azido (**2**) and cyanato (**3**) ions. The only previously reported examples of such bridging by azides are the cobalt(II)[12] and nickel(II)[14] analogues of **2**, while this is the first occurrence of such bridging by cyanates.

As far as iron(II) chemistry is concerned, the reported examples of bridging pseudohalido complexes are very rare. They include discrete dinuclear or tetranuclear $\mu_{1,1}$-azido- or cyanato-bridged species,[20] a 2D $\mu_{1,1}$-N_3-bridged layered complex,[27] and 2D ($\mu_{1,3}$-N_3) or 1D ($\mu_{1,1}$-N_3 and $\mu_{1,3}$-N_3) coordination polymers.[28] Thus, complexes **2** and **3** are the first two examples of the $\mu_{1,1,1,1}$ bridging mode in iron(II) chemistry.

A close examination of the eight octahedrally coordinated iron(II) ions in complexes **1–3** reveals the existence of two bonds in *trans* positions that are significantly shorter than the other four, thus forming a compression axis (see Tables S1–S3 in the Supporting Information).

The enneanuclear molecules of **1–3** are well separated from each other, with the closest intermetallic distances being about 8 Å.

Static magnetic properties: $\chi_M T$ versus T data for complexes **1–3** are shown in Figure 3. The $\chi_M T$ product for complex **1**, under a field of 1 T, is 29.0 $cm^3 mol^{-1} K$ at 300 K and remains almost constant upon cooling to about 100 K (with a broad and shallow maximum of 29.2 $cm^3 mol^{-1} K$ at 176 K), and then drops to 4.8 $cm^3 mol^{-1} K$ at 2 K (Figure 3). This drop is associated with a partial depopulation of higher spin states and zero-field splitting effects. The susceptibility does not extrapolate to zero as the temperature tends to zero, suggesting a magnetic ground state.

For complex **2**, under a field of 0.1 T, the $\chi_M T$ product increases smoothly from 31.8 $cm^3 mol^{-1} K$ at 300 K to a maximum of 59.0 $cm^3 mol^{-1} K$ at 19 K and then drops suddenly to 26.3 $cm^3 mol^{-1} K$ at 2 K. This maximum indicates dominant ferromagnetic interactions within the cluster, whereas the sudden drop at low temperatures may be associated with

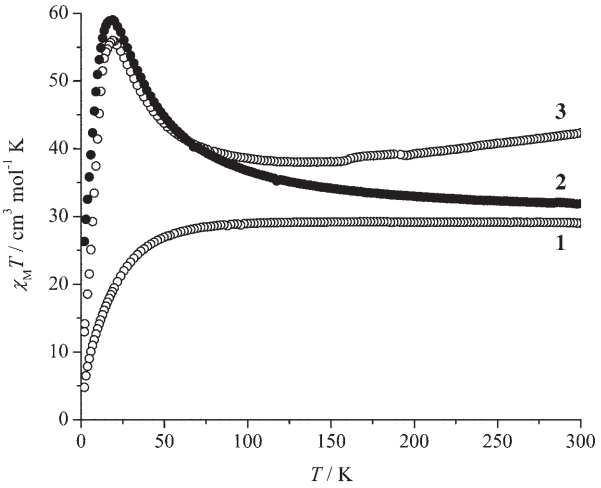

Figure 3. Magnetic susceptibility data for **1**–**3** (under an applied magnetic field of 1 T for **1** and 0.1 T for **2**, **3**) shown as $\chi_M T$ versus T plots.

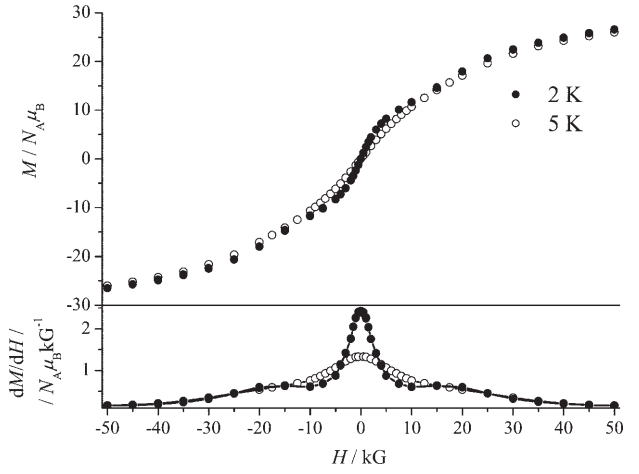

Figure 4. Magnetization M of complex **2** as a function of the applied magnetic field H over the ± 5 T range (top). Steps in the magnetization are illustrated by the appearance of shoulders in the dM/dH versus H plot around ± 2 T (bottom).

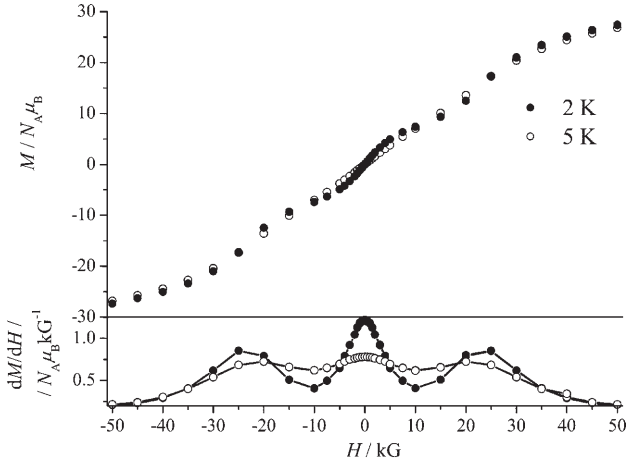

Figure 5. Magnetization M of complex **3** as a function of the applied magnetic field H over the ± 5 T range (top). Steps in the magnetization are illustrated by the appearance of peaks in the dM/dH versus H plot around ± 2.5 T (bottom).

zero-field splitting effects. The maximum is field-dependent, being compressed and shifted to higher temperatures as the field is increased (see Figure S2 in the Supporting Information). This may be attributed to the additional splitting of Zeeman levels by the applied magnetic field.

The situation is similar for complex **3**, with a $\chi_M T$ value of 42.3 cm^{3}mol^{-1}K at 300 K dropping to a broad minimum of 38.0 cm^{3}mol^{-1}K at 132 K and rising to a field-dependent maximum of 56.0 cm^{3}mol^{-1}K at 19 K (0.1 T). The subsequent sudden drop to 13.0 cm^{3}mol^{-1}K at 2 K is associated with zero-field splitting effects (see Figure S3 in the Supporting Information). Increasing the field up to 5 T leads to a decrease in the maximum and a shift to higher temperatures due to a stronger splitting of the Zeeman levels (see Figure S3 in the Supporting Information). Due to the large nuclearity of these clusters and the orbital degeneracy of iron(II) ions, the data for **1**–**3** could not be modeled.

Additional magnetization measurements were carried out as a function of the applied magnetic field, in order to further probe the nature of the ground states of **2** and **3**. Magnetization isotherms of complex **2** show that there is no saturation up to 5 T at 2 K (Figure 4). At 5 T, the magnetization reaches 26.2 $N_A\mu_B$ (2 K), a value lower than the theoretically expected one (28.00 $N_A\mu_B$) for an $S=14$ spin of the ground state ($g=2$), but slightly above the value for an $S=13$ spin. A theoretical curve based on a spin Hamiltonian assuming an $S=14$ value and including ZFS terms does not satisfactorily reproduce the experimental curve. This behavior strongly suggests that several states are thermally populated at 2 K, contributing in a rather complicated manner to the magnetization of the system. The situation is similar in the case of complex **3** (Figure 5), for which the magnetization does not reach saturation under a field of 5 T at 2 K: the value of 27.4 $N_A\mu_B$ attained is intermediate between those predicted for $S=13$ and $S=14$ spin states.

A prominent feature of the magnetization isotherms, and especially of that at 2 K, is the appearance of a step at around 2.5 T, which may be attributed to crossings of the energy levels as a function of the applied magnetic field. We assume that this behavior is analogous to that previously described for a decanuclear ferric wheel[29] and more recently for a diferric complex.[30] It is likely that additional, sharper steps would have been visible at lower temperatures, but these were unfortunately inaccessible with our facility. The high reactivity of our complexes towards atmospheric oxygen and the ease with which solvent loss occurs complicate subsequent measurements with other techniques (such as micro-SQUID) in the mK range.

To further probe the ground states of **2** and **3**, M versus HT^{-1} plots in the range 2–10 K were constructed under applied magnetic fields of 0.1, 0.5, 1, 2.5, and 5 T (data not shown). Supposing that over this temperature range essentially only the ground state is populated, fits were carried out considering an isolated spin S with single-ion parameters of g and D. When a collective spin S is considered for all

magnetic fields, the calculated curves severely overestimate the low-field data and underestimate the high-field data. Clearly, considering a single, isolated ground state for all applied fields is not a valid approximation. We were thus unable to unequivocally determine the ground states of the complexes.

However, in order to derive a qualitative estimate of the ground-state properties, zero-field measurements were carried out by means of AC susceptometry. The $\chi_M'T$ versus T data are linear below 5 K for both complexes. Extrapolation to 0 K and assumption of Curie law behavior at this temperature can be used to probe the ground state of the complex at zero field. The $\chi_M'T$ value for **2** at 0 K is ~20.5 $cm^3 mol^{-1} K$, corresponding to an $S=6$ spin ($g=2$), while the value for **3** is ~7.5 $cm^3 mol^{-1} K$, corresponding to a spin value between 3 and 4 ($g=2$). These estimations were based on the assumption that $g=2.0$; in the case of iron(II) ions, this value may be slightly larger, thus complicating the estimation of S.

It is clear from the above that it is not possible to obtain a quantitative picture of the electronic structures of the complexes due to computational limitations (for full-matrix calculations) and the limitations of the theoretical models employed (HDvV approach). However, some qualitative points are clear: i) complex **1** has an electronic structure that is significantly different from those of complexes **2** and **3**, with the latter exhibiting higher ground spin states; ii) this difference in electronic structure may be attributed to the different monoatomic bridges of the complexes (μ_4-OH^- for **1** versus μ_4-N_3^- for **2** and μ_4-NCO^- for **3**), which result in different coupling interactions.

Dynamic magnetic properties: Analysis of their static magnetic susceptibility data strongly suggests that complexes **2** and **3** are characterized by relatively high ground spin states associated with appreciable anisotropy. These properties are prerequisites for single-molecule magnet behavior. Therefore, we examined their dynamic magnetic properties by AC magnetic susceptibility measurements over the temperature range 1.9–5.0 K, applying a weak (10^{-4} T) alternating magnetic field oscillating at frequencies of 1, 5, 10, 50, 100, 250, 500, and 1000 Hz under zero static magnetic field.

The compounds exhibit in-phase (χ_M') and out-of-phase (χ_M'') magnetic susceptibility signals, below 3.5 K for **2** (Figure 6) and below 4 K for **3** (Figure 7), due to their inability to relax rapidly enough to keep up with the oscillating field at these temperatures. The frequency dependence of the χ_M'' signals clearly indicates slow magnetic relaxation effects, as is to be expected for SMM behavior. As determined by fits to Lorentzian lines, the χ_M'' peak of **2** shifts from 2.34(9) to 2.00(10) K upon decreasing the frequency of the AC field from 1000 to 50 Hz; at lower frequency, it is shifted below 1.9 K and is thus no longer visible. For **3**, the χ_M'' peak shifts from 2.77(6) K to 2.08(6) K upon decreasing the frequency of the AC field from 1000 to 5 Hz; at lower frequency, it is shifted to below 1.9 K and is thus no longer visible.

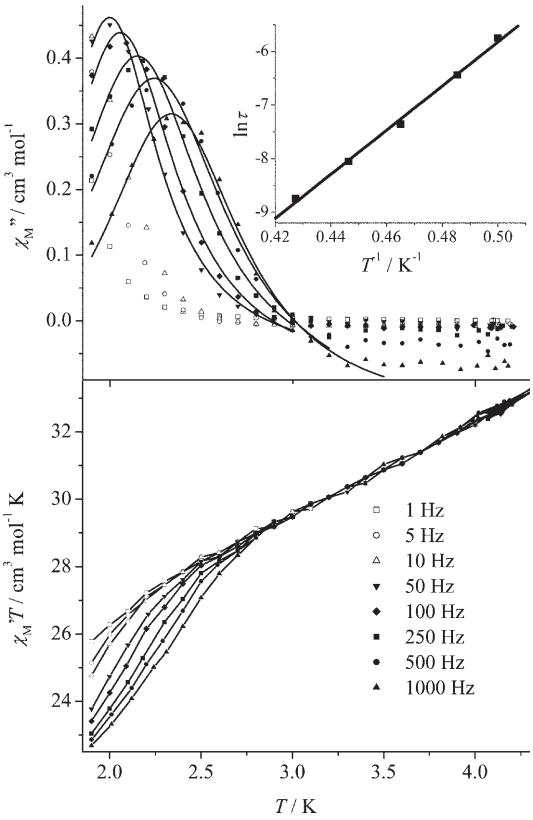

Figure 6. Frequency dependence of the in-phase $\chi_M'T$ product and out-of-phase χ_M'' magnetic susceptibility versus T for complex **2**. Solid lines are fits of the out-of-phase experimental data by Lorentzian lines. An Arrhenius plot of $\ln\tau$ versus T^{-1} for the values derived from the peak maxima at various frequencies is shown in the inset. The solid line is a least-squares linear fit of the data. Attempts to fit the curves for which the χ_M'' versus T maxima are not observable (1, 5, 10 Hz) were unsuccessful.

The magnetization relaxation rate data obtained from the AC data were fitted to the Arrhenius equation $\tau=\tau_0 \exp(U_{eff}/kT)$, where τ is the relaxation time, U_{eff} is the effective energy barrier for the relaxation of the magnetization, k is Boltzmann's constant, and τ_0 is a pre-exponential factor. From the fits, U_{eff} was found to be 29(1) cm^{-1} (41(1) K) with $\tau_0=3.4\times10^{-12}$ s for **2**, and 30(1) cm^{-1} (44(1) K) with $\tau_0=2.0\times10^{-11}$ s for **3**. Comparison of the data obtained for the two complexes clearly shows that the SMM behavior is manifested at a lower temperature for **2** (3 K) than for **3** (3.5 K). This difference in relaxation behavior may be primarily attributed to the pre-exponential factor of complex **3**, which is about an order of magnitude larger than that of complex **2**, rather than to its marginally higher thermodynamic barrier.

The out-of-phase signal is stronger in the case of **3**, with the χ_M''/χ_M' ratio reaching 0.11 (2.10 K, 50 Hz), whereas for complex **2** the respective value does not exceed 0.036 (2.00 K, 50 Hz). The ratio χ_M''/χ_M' for both compounds is rather small in comparison with the values for other single-molecule magnets. However, this is not unprecedented in the literature as many compounds exhibiting SMM behavior have low χ_M''/χ_M' ratios.[31,32] With regard to dynamic magnetic properties, it is generally assumed that the samples are

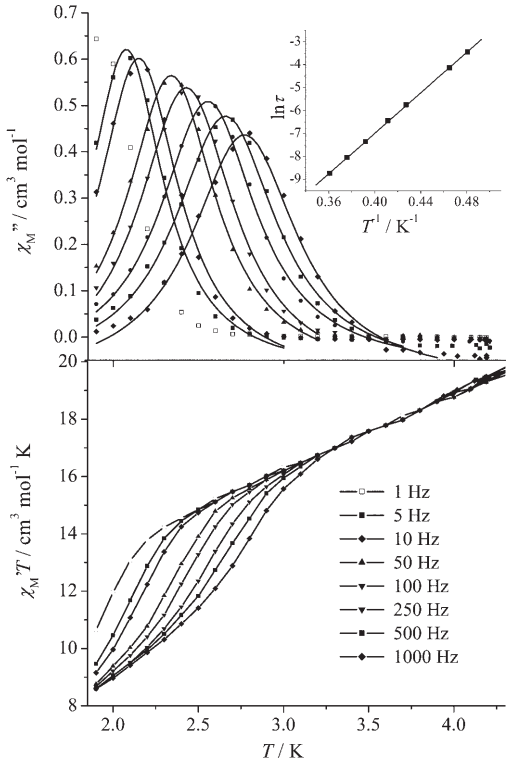

Figure 7. Frequency dependence of the in-phase $\chi_M'T$ product and out-of-phase χ_M'' magnetic susceptibility versus T for complex **3**. Solid lines are fits of the out-of-phase experimental data by Lorentzian lines. An Arrhenius plot of $\ln\tau$ versus T^{-1} for the values derived from the peak maxima at various frequencies is shown in the inset. The solid line is a least-squares linear fit of the data. Attempts to fit the curve for which the χ_M'' versus T maximum is not observable (1 Hz) were unsuccessful.

characterized by inhomogeneities, with one part undergoing slow relaxation and another part undergoing fast relaxation.[18] In the present cases, we have established that the electronic structures of the ground states are rather complicated. From the M versus H experiments at low temperatures, it became apparent that the ground states of these systems could not be characterized by a well-defined spin with an effective zero-field splitting D to which an energy barrier could be directly assigned. This implies that low-lying spin states are occupied in the 2–4 K temperature range. These low-lying excited spin states may not fulfill the conditions for slow relaxation. Low-lying spin states may also provide alternative pathways for thermally assisted relaxation of magnetization, thus leading to a rather small pre-exponential factor.

Mössbauer spectroscopy: The Mössbauer spectra of **1** and **3** were recorded between 1.8 and 293 K, and that of **2** between 1.8 and 260 K. In all cases, the spectra above ~12 K show two well-resolved quadrupole-split doublets with parameters typical of high-spin iron(II). The molecular structures of the complexes suggest the presence of two iron(II) sites giving rise to peaks in an 8:1 relative area ratio, corresponding to the eight external octahedrally coordinated and the one central octacoordinate iron(II) ion, respectively. Moreover, of the two sites, comprising the FeO_5N (**1**) or FeO_4N_2 (**2** and **3**) and FeO_8 chromophores, respectively, we would expect a higher isomer shift, δ, for the FeO_8 site. Finally, because the distortion from octahedral geometry is more pronounced for the octacoordinated site, we would also expect a higher quadrupole splitting ΔE_Q for this site. Indeed, the good separation of the two doublets allowed us to fit the spectra without any constraints. The results were in perfect agreement with the above reasoning (Table 1).

Table 1. Characteristic Mössbauer parameters for **1**–**3** at 78 K.

Complex	Site	δ [mm s^{-1}]	ΔE_Q [mm s^{-1}]	$\Gamma/2$ [mm s^{-1}]	Area [%]
1	I	1.23	2.61	0.18	89
	II	1.35	3.18	0.14	11
2	I	1.20	2.42	0.16	87
	II	1.37	3.10	0.12	13
3	I	1.16	2.40	0.16	89
	II	1.34	3.15	0.12	11

Representative Mössbauer spectra of **1**–**3** at 78 K are shown in Figure 8. The appearance of the spectra remains essentially unchanged over the whole 293–15 K range, with just a relative broadening of the lines at lower temperatures and an increase in the isomer shifts upon cooling to ~78 K due to second-order Doppler effects.[33] The sharpness of the spectra at this temperature is noteworthy, indicating a well-defined environment for the iron(II) sites of the three complexes.

The quadrupole splitting for the minor Fe^{II} site of each complex exhibits little temperature dependence. The major

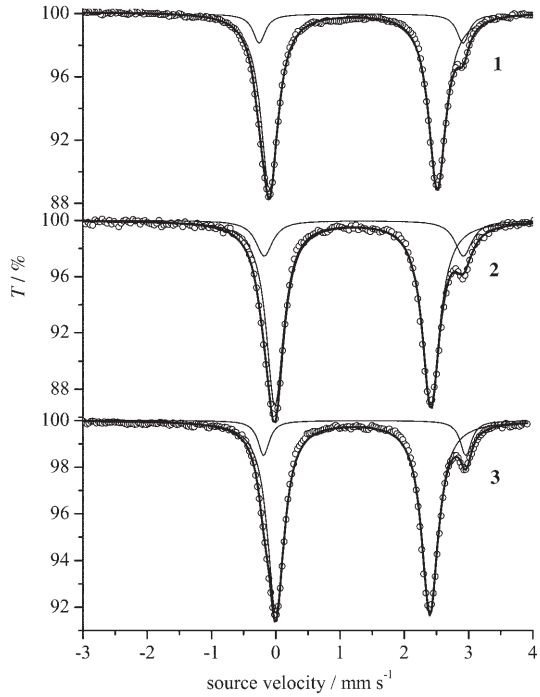

Figure 8. Mössbauer spectra of **1**–**3** at 78 K, and their fit to two quadrupole-split doublets (fitting parameters in Table 1).

site shows a marked decrease in ΔE_Q upon heating, mainly above liquid nitrogen temperature. This variation is only 1–2% for the minor site between 78 and 300 K, but amounts to 10% for the major site in the same temperature range (Figure 9). This suggests the existence of low-lying excited orbital states for these sites, which become thermally populated at higher temperatures. This casts doubt on the validity of the isotropic exchange Hamiltonian.

Figure 10, as well as Figure S4 and Figure S5 in the Supporting Information show Mössbauer spectra recorded from powdered samples of **1**–**3** near liquid helium temperatures. These low-temperature spectra reveal the onset of slow relaxation effects for all

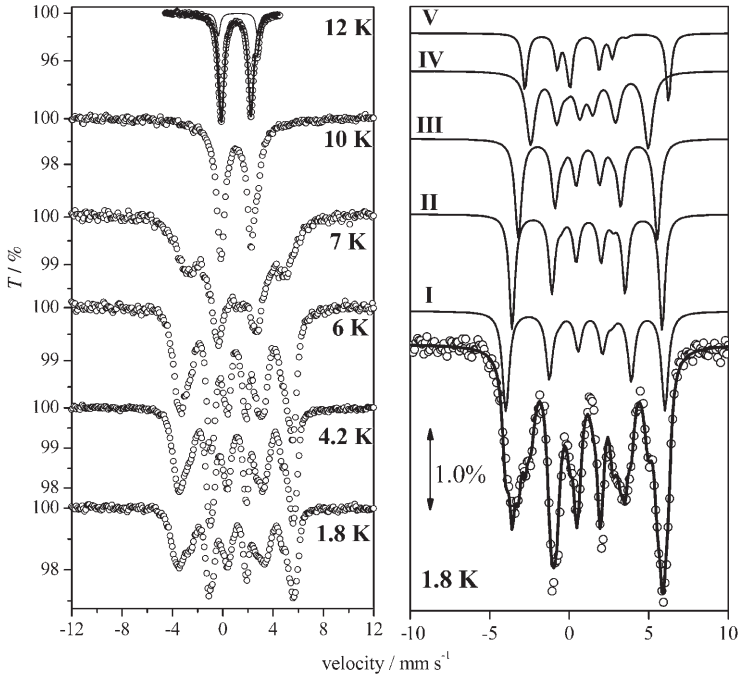

Figure 10. Low-temperature Mössbauer spectra of **3**. The 1.8 K spectrum has been fitted according to the assumptions described in the text.

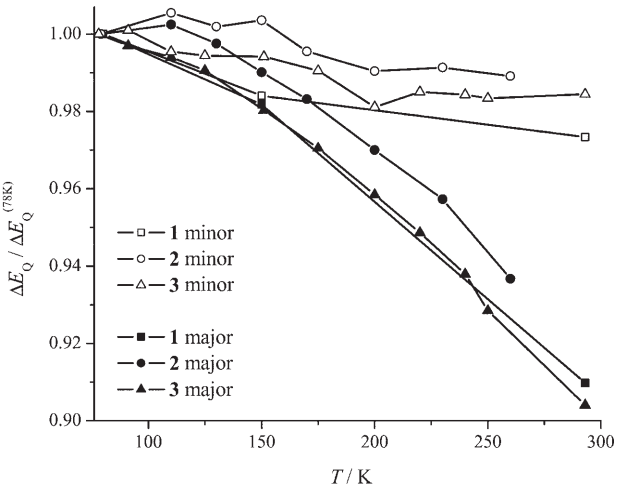

Figure 9. Thermal variation of the $\Delta E_Q/\Delta E_Q^{(78\,K)}$ ratio for both sites of **1**–**3**. Minor and major sites are shown with open and filled markers, respectively.

three complexes. Well-resolved hyperfine magnetic spectra are obtained at 1.8 K for **1** and at 4.2 and 6.5 K for **2** and **3**, respectively. The characteristic timescale of Mössbauer spectroscopy is of the order of 10^{-8} s, and therefore this technique may be used to monitor the dynamic behavior of the spins in a different window to AC susceptometry. The appearance of intermediate relaxation in the 4.2–10 K temperature range for **2** and **3** is consistent with the AC susceptibility measurements. Extrapolation of the Arrhenius law in this temperature range, with the parameters derived from AC susceptometry (see above), indicates that the relaxation times are in the range of 6×10^{-8} to 2×10^{-10} s for **2** and 7.0×10^{-7} to 2.0×10^{-9} s for **3**. Also consistent with the above picture is the fact that the relaxation effects start at a higher temperature for **3** than for **2**. The observation of magnetically split spectra in the absence of an external magnetic field indicates that the low-lying states of the complexes consist of almost degenerate non-Kramers doublets with Ising-type anisotropy. This is at variance with the usual Mössbauer spectra of complexes characterized by singlet spin states of Fe^{II}, which show quadrupole-split doublets.[34]

The observation of magnetically split Mössbauer spectra for complex **1** is noteworthy. A fully magnetically split spectrum is observed at 1.9 K, whereas at 4.2 K the spectrum exhibits complicated behavior (see Figure S4 in the Supporting Information). The observation of a magnetically split spectrum at zero field at the lowest temperature indicates that the ground state of **1** also consists of an almost degenerate non-Kramers doublet. Because of the small nominal spin of the ground state of **1**, its dynamic behavior was not studied further.

Figure 10, as well as Figure S4 and Figure S5 in the Supporting Information also show theoretical simulations of the 2 K spectra for the three compounds. In order to reproduce each spectrum, we proceeded as follows: i) a simple model was applied assuming that each iron nucleus experiences a magnetic field B_i with a fixed orientation relative to the largest component of an axial ($\eta=0$) electric field gradient tensor; ii) on the basis of the $T>20$ K spectra, we assumed two different groups of ferrous sites in terms of δ and ΔE_Q values, and these parameters were kept constant during the

fitting procedure; iii) one ferrous site was assigned to the central iron atom, while the site corresponding to the remaining eight iron atoms was progressively subdivided from one to two and then to four ferrous subsites (with relative values of 8, 4, and 2, respectively, compared to the central site); iv) the line-widths $\Gamma_{1/2}$ were left as free variables.

The best results were obtained by assuming five magnetically distinct species in a 2:2:2:2:1 ratio. This model suggests that the eight hexacoordinate ferrous atoms can be grouped into four subsites (I–IV). The results of the fits are listed in Table 2.

Table 2. Mössbauer parameters obtained from fitting the 2 K spectra of compounds **1–3** as described in the text.

Complex	Site	B_i [T]	θ [°][a]	Γ [mm s^{-1}]
1	I	32.5	75	0.60
	II	29.8	72	0.70
	III	28.8	57	0.94
	IV	10.3	60	1.98
	V	24.5	33	0.73
2	I	30.4	76	0.82
	II	28.4	60	0.48
	III	25.5	57	0.50
	IV	19.7	41	0.48
	V	24.0	41	0.48
3	I	28.3	63	0.53
	II	26.2	57	0.45
	III	23.8	55	0.50
	IV	19.2	53	0.73
	V	22.4	34	0.38

[a] θ is the angle between the internal magnetic field, B_i, and the direction of the largest component of the EFG tensor.

The magnetic field B_i at each ferrous site depends on the exchange coupling between these sites according to the relationship:

$$B_i = B_0\langle S_i\rangle/S \quad (3)$$

where B_0 is the intrinsic field at each ferrous site. The intrinsic magnetic field B_0 is the sum of the Fermi contact term B_F, which is isotropic and negative, the orbital term B_L, which is isotropic and positive, and the dipolar term B_D, which is anisotropic.[35] For high-spin iron(III) complexes, only the B_F term is important, resulting in a rather simple situation. For high-spin iron(II) complexes, however, B_L and B_D contribute significantly and B_0 cannot be reliably estimated. $\langle S_i\rangle$ is the spin expectation value for each ferrous site and S is the total spin. If we assume that B_0 is common to all of the ferrous sites, then the magnetic inequivalence between these sites must be due to different $\langle S_i\rangle$ values. This parameter critically depends on the coupling scheme.[36] From Table 2, it can be seen that all ferrous sites are characterized by appreciable magnetic fields, indicating that considerable spin density is located on each site. This indicates that the spin of the ground state results from a non-trivial spin-coupling mechanism, in agreement with the magnetic susceptibility data, which were indicative of intermediate spin for the ground state. We may rule out cases in which intermediate couplings between individual sites i and j are such that $S_{ij}=0$. In this event, we would expect sites with negligible $\langle S_i\rangle$ values, leading to cancellation of the internal magnetic fields.

It is useful to compare the dynamic magnetic behavior as monitored by AC susceptibility measurements and the Mössbauer properties of the present compounds **1–3** with those of some iron(III) complexes exhibiting SMM behavior.[32g,37,38] In the cases of "Fe8"[37] and "Fe4",[38a] the ground state of the systems is characterized by a well isolated spin ($S=10$ and $S=5$, respectively) and the relaxation of magnetization follows the Arrhenius law with a pre-exponential factor of 10^{-7} s and an energy barrier of 22 K. This energy barrier is smaller in comparison with those of complexes **2** and **3**. However, the pre-exponential factors for **2** and **3** are four to five orders of magnitude smaller than those for "Fe4" and "Fe8". This difference in pre-exponential factors is reflected in the temperature ranges over which relaxation phenomena are observed by Mössbauer spectroscopy. For the "Fe4" and "Fe8" clusters, these effects appear at temperatures above 30 K, whereas for the present clusters **1–3**, relaxation spectra are observed at $T<12$–13 K. For the Fe13 cluster,[32g] an energy barrier of about 13 K and a rather small pre-exponential factor of 10^{-13} s have been derived from AC susceptibility data, and magnetically split spectra emerge at $T<13$ K.

Concerning SMMs based on high-spin ferrous ions, of relevance are the alkoxo-bridged ferrous cubes.[16,17] However, no Mössbauer spectra are available for these. Their pre-exponential factors were found to be $\sim 10^{-9}$ s, with energy barriers of 26–30 K. With these values, we would expect relaxation effects in the Mössbauer spectra to emerge in the range 10–15 K. Two other similar alkoxo-bridged ferrous cubes have been reported.[39] One of them was shown to exhibit an $S=8$ ground state, but the dynamic magnetic properties were not reported. However, the zero-field Mössbauer spectra at 4.2 K comprise a quadrupole-split doublet. The results of the present study strongly suggest that the lack of magnetically split Mössbauer spectra at this temperature disfavors the likelihood that this compound may exhibit SMM behavior. Either the ground state of this compound is a singlet, which does not exhibit uniaxial properties, or the relaxation times are fast ($t<10^{-8}$ s at 4.2 K), thus precluding superparamagnetic behavior. For the other complex, the static magnetic measurements were complicated and no analysis was pursued,[40] and the dynamic magnetic properties were not monitored. Solid samples of this cluster exhibited magnetically split Mössbauer spectra without an applied magnetic field at $T<\sim 6$ K, but this behavior was attributed to low-dimensional intermolecular interactions.

X-band EPR spectroscopy: Figure 11 shows the X-band EPR spectra of powdered samples of complexes **1–3** recorded at 4.2 K. As can be seen, a strong signal is observed for **1** at relatively low values of the external magnetic field, whereas **2** and **3** are EPR-silent. The results from Mössbauer

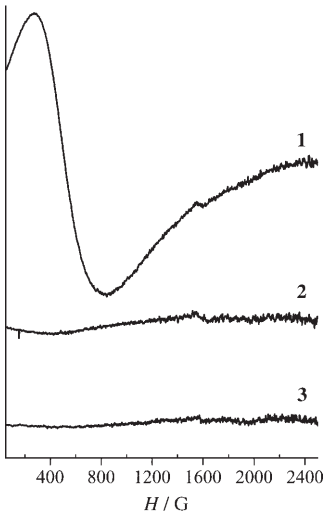

Figure 11. X-band EPR spectra of powdered samples of **1**–**3** at 4.2 K. *EPR conditions:* microwave power 38 mW, mod. ampl. 25 Gpp, microwave frequency 9.40 GHz (perpendicular mode).

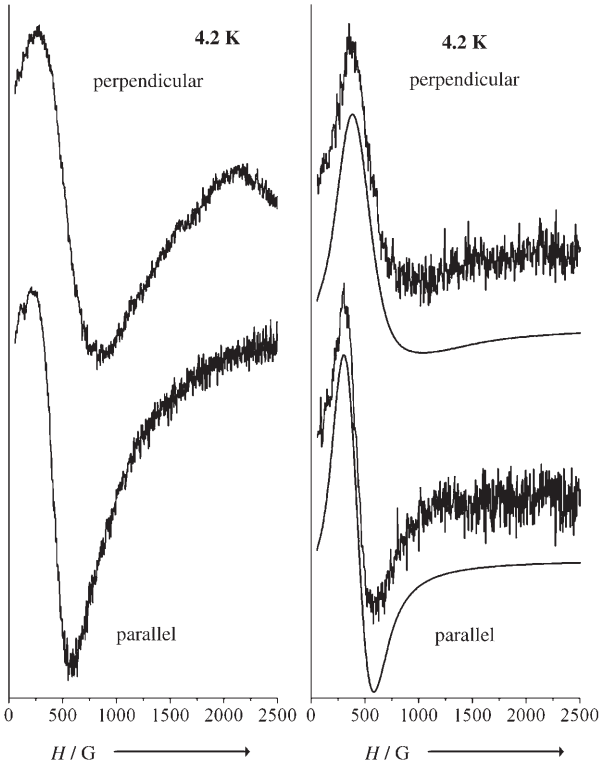

Figure 12. Perpendicular (top) and parallel-mode (bottom) X-band EPR spectra for complex **1**, at 4.2 K in the solid state (left) and in frozen toluene solution (right). The solid lines are simulations of the spectra considering transitions obeying Equation (4) with $\Delta_0 = 0.28\ cm^{-1}$, $g_{eff} = 8.0$, and $\sigma\Delta_0 = 0.025\ cm^{-1}$. *EPR conditions:* microwave power 38 mW, mod. ampl. 10 Gpp, microwave frequency 9.35 GHz (parallel mode), 9.60 GHz (perpendicular mode).

spectroscopy presented above indicate that the ground states of **2** and **3** are almost degenerate non-Kramers doublets. Intra-doublet X-band EPR signals are expected from such systems, provided that the inter-doublet separation Δ_0 at zero field is finite, of the order of microwave energy ($h\nu \sim 0.3\ cm^{-1}$). If $\Delta_0 \ll h\nu$, the transition probability is small. The absence of X-band EPR signals for **2** and **3** at 4.2 K is in agreement with the Mössbauer spectroscopy results discussed above, which indicate that $\Delta_0 \sim 0$.

The line shape of the EPR spectrum of **1** is strongly reminiscent of signals usually observed for integer spin systems.[40] In general, these signals are retained and enhanced when the EPR experiment is carried out with the microwave field oscillating parallel to the external static magnetic field (parallel mode). Figure 12 shows EPR spectra of samples of **1**, powdered or dissolved in toluene, recorded in either perpendicular or parallel mode. The solid-state and solution spectra are similar, except that the features in the latter are slightly narrower.

Such integer spin signals are generated by microwave transitions between a pair of levels in a spin multiplet with a splitting Δ_0 in zero field that satisfies the condition $\Delta_0 < h\nu$. Because the pair of levels is not degenerate in zero field, a magnetic field will increase the splitting of the levels quadratically.[40] The resonance condition for such a non-Kramers doublet is given by Equation (4):

$$h\nu = \sqrt{\Delta_0^2 + (g_{eff}\beta \mathrm{H})^2} \qquad (4)$$

where g_{eff} is an effective g value.

The solution spectra in both parallel and perpendicular mode can be simultaneously simulated by assuming such a non-Kramers doublet.[40] Indicative (but not unique) parameters with which the spectra are well reproduced are $\Delta_0 = 0.28\ cm^{-1}$ and $g_{eff} = 8.0$. To reproduce the line shape, a Gaussian distribution of the parameter Δ_0 was employed, with $\sigma\Delta_0 = 0.025\ cm^{-1}$ (Figure 12).

Because of the complicated spin-coupling schemes for complexes **1**–**3**, further analysis and studies by X-band EPR spectroscopy were not pursued. A notable observation is that complexes **2** and **3** do not give rise to intra-doublet X-band EPR signals, which may be attributed to negligible Δ_0 values for each of the doublets occupied at 4.2 K. Since this parameter is a measure of quantum tunneling of magnetization,[41] a vanishingly small value indicates that this mechanism is not effective for **2** and **3**, as befits their slow relaxation properties.

High-field EPR studies, as well as other paramagnetic resonance techniques such as frequency domain magnetic resonance spectroscopy, are usually applied in order to quantitatively determine the spin and the zero-field splitting parameters for systems with well-isolated ground states and large spins.[42] In the present case, the complicated nature of the ground state, as revealed by the data presented herein, along with the high reactivity of the complexes towards atmospheric oxygen, give rise to theoretical and technical complications that preclude such studies for the time being.

^{1}H NMR spectroscopy: The ^{1}H NMR spectra of **1**–**3** were recorded in CD_3CN in order to assess the stability of these complexes in solution. This choice of solvent was based on the fact that all three complexes were initially prepared in acetonitrile. Assuming that the molecular structure (virtual D_{4h} symmetry) is retained in solution, we would expect five signals, four from the aromatic pyridyl protons and one from the acetate methyl protons, in a respective 1:1:1:1:3 ratio. In the case of **1**, the signals of the two hydroxo groups would be expected to be too broad and shifted to be observed.

The ^{1}H NMR spectrum of complex **1** shows broad and shifted peaks, spanning the $\delta = 0$–50 ppm range, characteristics that are typical of the NMR spectra of paramagnetic species and that are consistent with the high-spin ($S = 2$) electronic configuration deduced for the Fe^{II} ions in these complexes. The spectrum comprises a group of four broad and overlapping peaks in the $\delta = 47$–44.8 ppm range and an additional signal at $\delta = 37.6$ ppm (Figure 13 and Table 3). Careful integration of the peaks shows that the relative area ratio between the group of peaks at $\delta = 47.0$, 46.2, 45.5, and 44.8 ppm and the peak at $\delta = 37.6$ is 1.1:1, close to the value of 1.3:1 expected for the H_{py}:H_{ac} ratio. This rules out the possibility that the less shifted peak might be assigned to a pyridyl proton, which would require a 3:1 relative area ratio. Thus, the less shifted peak is assigned to the protons of the coordinated acetato ligand and the group of four overlapping peaks is assigned to the pyridyl protons.

The spectra of complexes **2** and **3** are almost identical. They span the $\delta = 0$–60 ppm range and feature four broad but discrete peaks in the $\delta = 35$–60 ppm range, with three peaks in the $\delta = 42$–58 ppm range almost equal in intensity and a much more intense peak at around $\delta = 40$ ppm (Figure 13 and Table 3). Careful integration confirms an approximate ratio of 1:1:1:3 between the more shifted triad and the less shifted peak. This leads us to assume that only three of the pyridyl protons are observable, with the signals of those adjacent to the paramagnetic center (6,6′) being too broad and shifted. This is a characteristic attribute of pyridyl protons close to paramagnetic centers, and has been observed for the 2,9-protons of 1,10-phenanthroline and the 6,6′-protons of 2,2′-bipyridine[43] in their respective iron(III) complexes, the signals of these protons being significantly shifted and appearing as very broad peaks. The overall appearance of the spectra indicates the absence of equilibria in solution. Thus, we attribute the first three peaks to three pyridyl protons and the less shifted peak to the acetato protons.

Table 3. ^{1}H NMR shifts for complexes **1**–**3**.

Complex	Pyridyl protons	Methyl protons
1	47.0, 46.2, 45.5, 44.8	37.6
2	57.2, 52.5, 45.9	41.0
3	54.6, 51.4, 44.4	39.9

For all three complexes, an unequivocal assignment of the observed pyridyl signals is not yet possible. For this, further experiments would be necessary, but the absence of cross-peaks in the 2D COSY and TOCSY spectra deterred us from carrying out additional studies.

An important feature of the ^{1}H NMR spectra of complexes **1**, **2**, and **3** shown in Figure 13 is that two of the pyridyl protons of complexes **2** and **3** show larger chemical shift differences ($\Delta\delta \sim 7$ ppm) compared to the respective protons of **1** ($\Delta\delta \sim 3$ ppm). In addition, one of the proton signals observed in the spectrum of **1** (6,6′) is not observed in the spectra of **2** and **3** due to a strong paramagnetic shift. Making the reasonable assumption that these three complexes adopt almost identical structures in solution, as in the solid state, these differences can only be attributed to the different electronic structures stemming from different coupling of the spins. At 298 K, a multitude of electronic states is thermally populated. Due to the different couplings within **1** as compared to those within **2** and **3**, the mapping of these electronic states is expected to differ, thereby resulting in differences in the paramagnetic NMR shifts.

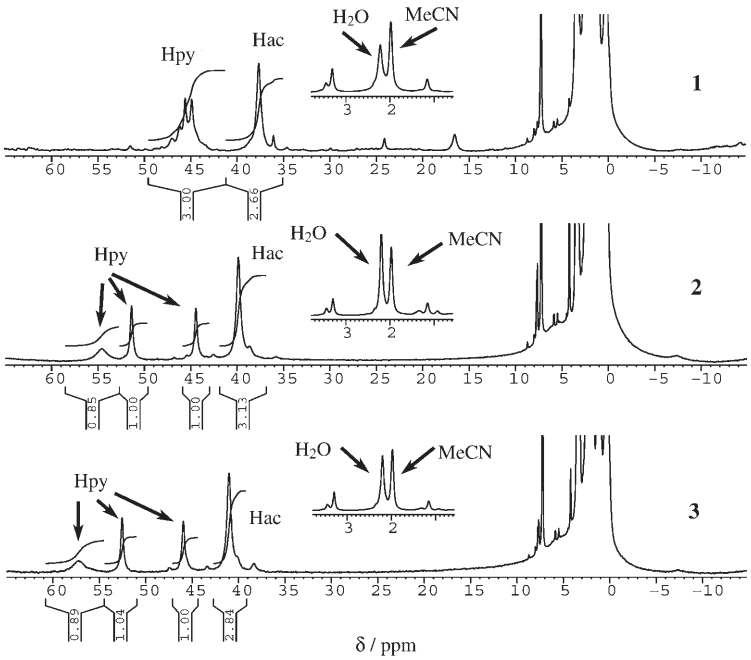

Figure 13. ^{1}H NMR spectra of complexes **1**, **2**, and **3** in CD_3CN. The aromatic and acetato protons show strong paramagnetic shifts and line broadenings. The expansion of the diamagnetic region shows the presence of solvent impurities, as well as some acetato protons.

Conclusion

In the present work we have made use of prior synthetic and physical knowledge to design and synthesize new single-molecule magnets: complexes **1–3** have been prepared according to synthetic methods that have previously been used to obtain the respective Co^{II} and Ni^{II} complexes, and their stability in solution has been verified by ^1H NMR spectroscopy. Complexes **2** and **3** have been found to exhibit SMM behavior, as desired, but close-lying magnetic states lead to an undeterminable ground state. This leads to possible level crossings of the lowest-lying states upon application of varying magnetic fields and consequent stabilization of different ground states. Magnetic susceptibility results have been compared with ^{57}Fe Mössbauer and X-band EPR spectroscopic results. Mössbauer spectroscopy showed the onset of magnetic relaxation at different temperatures for the three complexes.

The combined examination of magnetic susceptibility, X-band EPR, and Mössbauer spectroscopic data has led to the conclusion that the electronic structures of **1–3** are too complicated to be simply described, mainly due to: i) non-negligible orbital contributions of the iron(II) ions, ii) proximity of the spin states due to moderate Fe^{II}–Fe^{II} exchange couplings, which results in a multitude of low-lying excited states that are progressively stabilized by increasing magnetic fields, and iii) magnetic inequivalence of the iron(II) sites. Some firm conclusions concerning their electronic structures can be drawn, but detailed descriptions are elusive. Thus, these systems present a challenge to the theory of molecular magnetism, being at the bordeline between tractable and intractable systems. They also constitute non-classical examples of SMMs, in the sense that their ground states are not well isolated and the energy barrier for spin reversal cannot be calculated from a simple $D\hat{S}_z^2$ Hamiltonian.

Experimental Section

Syntheses

Caution: *Although no such behavior was observed during the present work, azido salts are potentially explosive and should be handled with care.*

$[Fe_9(OH)_2(O_2CMe)_8\{(2\text{-py})_2CO_2\}_4]$ (1): Treatment of a white slurry of $Fe(O_2CMe)_2\cdot 1.75\,H_2O$ (0.411 g, 2.00 mmol) in MeCN (50 mL) with $(2\text{-py})_2CO$ (0.184 g, 1.00 mmol) resulted in the formation of a dark blue-green solution. The solution was boiled for 5 min, in the course of which a noticeable color change to dark red was observed. The red solution was filtered and allowed to stand undisturbed in a stoppered flask inside the glovebox. After 2–3 days, red cubes of $\mathbf{1}\cdot 6.67\,H_2O\cdot 2.67\,MeCN$ had formed. These were collected by filtration, washed with MeCN, and dried in vacuo. The yield was about 30%. The dried solid analyzed as solvent-free. Elemental analysis calcd (%) for $C_{60}H_{58}Fe_9N_8O_{26}$ (1809.8): C 39.82, H 3.23, N 6.19; found: C 39.74, H 2.93, N 5.96.

$[Fe_9(N_3)_2(O_2CMe)_8\{(2\text{-py})_2CO_2\}_4]$ (2) and $[Fe_9(NCO)_2(O_2CMe)_8\{(2\text{-py})_2CO_2\}_4]$ (3): Treatment of a white slurry of $Fe(O_2CMe)_2\cdot 1.75\,H_2O$ (0.657 g, 3.20 mmol) in MeCN (60 mL) with $(2\text{-py})_2CO$ (0.295 g, 1.60 mmol) resulted in the formation of a dark blue-green solution. The solution was boiled for 5 min, in the course of which a noticeable color change to dark red was observed, and then solid NaN_3 (0.052 g, 0.80 mmol) for **2** or KOCN (0.065 g, 0.80 mmol) for **3** was added. The orange-red solutions were left to cool, the respective precipitates of NaO_2CMe (**2**) and KO_2CMe (**3**) were filtered off, and the resulting solutions were allowed to stand in stoppered flasks inside the glovebox. After 2–3 days, orange prisms of $\mathbf{2}\cdot 1.36\,H_2O\cdot 2.16\,MeCN$ and yellow prisms of $\mathbf{3}\cdot 0.25\,H_2O\cdot 2.37\,MeCN$ had formed. These were collected by filtration, washed with MeCN, and dried in vacuo. The yields were about 40% for **2** and about 30% for **3**. The dried samples analyzed as solvent-free. Elemental analysis calcd (%) for **2** ($C_{60}H_{56}Fe_9N_{14}O_{24}$, 1859.8): C 38.75, H 3.04, N 10.54; found: C 38.60, H 2.97, N 10.44. Elemental analysis calcd (%) for **3** ($C_{62}H_{56}Fe_9N_{10}O_{26}$, 1859.8): C 40.04, H 3.04, N 7.53; found: C 39.92, H 2.95, N 7.46.

Crystallographic data collection and structure determination: For complexes **1** and **2**, the selected crystals (**1**: red prismatic block, $0.50\times 0.25\times 0.17\,mm^3$; **2**: red prismatic block, $0.50\times 0.37\times 0.30\,mm^3$) were mounted on an Oxford Diffraction Xcalibur diffractometer equipped with an Oxford Instruments Cryojet cooler device and examined with graphite-monochromated $Mo_{K\alpha}$ radiation ($\lambda = 0.71073$ Å).[44] Data were collected at 180 K for **1** and 160 K for **2** in four runs ($\varphi = 0°$, 90°, 180°, 270°) and with ω scans up to $\theta = 26°$. 96313 (**1**) [44266 (**2**)] reflections were collected, of which 5668 (**1**) [22953 (**2**)] were independent ($R_{int} = 0.1219$ (**1**) [0.0407 (**2**)]). The absorption correction coefficients were 1.226 (**1**) and $1.657\,mm^{-1}$ (**2**). The structures were solved by direct methods using SHELXS-97[45] and refined againsy F^2 by a full-matrix least-squares method using SHELXL-97[46] with anisotropic displacement parameters for all non-hydrogen atoms. Scattering factors were taken from the literature.[47]

For complex **3**, data were collected at 180 K from a yellow (see synthesis above) prismatic crystal ($0.37\times 0.25\times 0.20\,mm^3$) mounted on an IPDS STOE diffractometer using graphite-monochromated $Mo_{K\alpha}$ radiation ($\lambda = 0.71073$ Å). The final unit cell parameters were obtained by least-squares refinement of a set of well-measured reflections, and monitoring for crystal decay during the data collection did not reveal any significant fluctuations in the intensities. 61248 reflections were collected, of which

Table 4. X-ray crystallographic data for complexes **1–3**.

	$\mathbf{1}\cdot 6.67\,H_2O\cdot 2.67\,MeCN$	$\mathbf{2}\cdot 1.36\,H_2O\cdot 2.16\,MeCN$	$\mathbf{3}\cdot 0.25\,H_2O\cdot 2.37\,MeCN$
formula	$C_{65.34}H_{79.35}Fe_9N_{10.67}O_{32.67}$	$C_{64.32}H_{65.2}Fe_9N_{16.16}O_{25.36}$	$C_{66.74}H_{63.61}Fe_9N_{12.37}O_{26.25}$
Fw	2039.73	1973.12	1961.60
space group	tetragonal, *P4/nnc*	triclinic $P\bar{1}$	triclinic $P\bar{1}$
a [Å]	25.4603(12)	18.864(1)	18.797(2)
b [Å]	25.4603(12)	20.177(1)	20.135(2)
c [Å]	25.274(2)	21.752(1)	21.783(3)
α [°]	90	101.015(3)	100.916(13)
β [°]	90	97.572(3)	97.843(13)
γ [°]	90	90.730(3)	90.497(10)
V [Å^3]	16383(2)	8049.8(5)	8014(2)
Z	6	4	4
ρ_{calcd} [g cm^{-3}]	1.231	1.637	1.643
λ [Å]	0.71073	0.71073	0.71073
T [K]	180(2)	160(2)	180(2)
$\mu(Mo_{K\alpha})$ [cm^{-1}]	1.226	1.657	1.664
reflections measured/unique	96313/5668 (R_{int}=0.1219)	44266/22953 (R_{int}=0.0407)	61248/26578 (R_{int}=0.0434)
data with ($I > 2\sigma(I)$)	4395	18381	20334
$R_{1(obs,all)}$	0.1085, 0.1358	0.0467, 0.0599	0.0371, 0.0547
$wR_{2(obs,all)}$	0.2733, 0.3021	0.1132, 0.1206	0.0893, 0.0988

26578 were independent ($R_{int}=0.0434$); the absorption correction coefficient was 1.664 mm^{-1}. The structure was solved by direct methods using SHELXS-97 and refined by least-squares procedures on F^2 with SHELXL-97. All non-hydrogen atoms were refined anisotropically.

For all three complexes, all hydrogen atoms were placed in idealized positions using a riding model and their isotropic displacement factors, U_{iso}, were fixed at 1.2 or 1.5 times U_{eq} of their parent carbon atom. As regards to the solvents of crystallization, the two acetonitrile and five water molecules of **1**, four of the six acetonitrile and two of the four water molecules of **2**, and four of the six acetonitrile and two water molecules of **3** were assigned partial occupancies and refined anisotropically along with the other non-hydrogen atoms. Crystallographic data are compiled in Table 4.

CCDC-661342 and CCDC-661343 contain the supplementary crystallographic data for complexes **1** and **3**, respectively. These data can be obtained free of charge via www.ccdc.cam.ac.uk/data_request/cif.

Physical measurements: C, H, and N microanalyses were performed at the Microanalytical Laboratory of the Laboratoire de Chimie de Coordination in Toulouse, France. Infrared spectra (4000–400 cm^{-1}) were recorded from samples in KBr disks on a Perkin-Elmer Spectrum GX FT-IR spectrometer.

Mössbauer measurements were performed on a constant acceleration conventional spectrometer with a 50 mCi ^{57}Co source (Rh matrix). The absorber was a powdered sample enclosed in a 20 mm diameter cylindrical plastic sample holder, the size of which had been determined to optimize the absorption. In order to avoid oxidation of the sample, the sample holder was sealed with Araldite inside the glovebox. Variable-temperature spectra were obtained in the 1.9–293 K range by using Oxford cryostats equipped with an Oxford ITC4 servocontrol device (±0.1 K accuracy). The WMOSS (WEB Research, http://www.webres.com) or Recoil[48] program packages were used to fit the Mössbauer spectra. Isomer shift values (δ) are reported relative to iron foil at 293 K.

Variable-temperature (2–300 K) DC magnetic susceptibility data were collected from vacuum-dried samples of **1**–**3** using a Quantum Design MPMS SQUID magnetometer in a field of 1 T (**1**) and 0.1, 0.5, 1, 2.5, and 5 T (**2** and **3**). To avoid aerial oxidation, the samples were pressed into 3 mm diameter pellets inside the glovebox and sealed within gelatin capsules. The gelatin capsules were transferred directly from the glovebox to the SQUID magnetometer to minimize the risk of aerial oxidation. Data were corrected by applying the standard procedure for the contribution of the sample holder and the diamagnetism of the sample. Variable-temperature AC magnetic susceptibility data for complexes **2** and **3** were collected between 1.9 and 5.0 K, with the magnetic field oscillating at 1, 5, 10, 50, 100, 250, 500, and 1000 Hz with an amplitude of 10^{-4} T. Additional measurements (250, 400, 600, 800, and 1000 Hz) were carried out under static magnetic fields of 0.1 and 0.2 T to evaluate the effect of the magnetic field on the relaxation process.

X-band EPR measurements were carried out with a Bruker ER-200D spectrometer equipped with a Bruker dual-mode cavity, an Anritsu frequency counter, an NMR gaussmeter, and an Oxford ESR-9 cryostat. To avoid sample oxidation, the EPR tubes were prepared inside the glovebox and flame-sealed on a vacuum line. **Caution:** *Molten quartz generates large amounts of harmful UV radiation and appropriate protective glasses must be worn to avoid eye-damage.* The spectra were simulated with software (SpinCount) kindly provided by Prof. M. Hendrich, Department of Chemistry, Carnegie Mellon University, Pittsburgh, PA, USA.

^1H NMR spectra were recorded from samples dissolved in CD_3CN at 293 K on a Bruker AMX400 spectrometer equipped with a 5 mm triple-resonance inverse probe operating at 400.13 MHz. ^1H chemical shifts are quoted relative to TMS using the residual protons of the solvent as a secondary standard. To avoid sample oxidation, CD_3CN was deoxygenated by repeated freeze-pump-thaw cycles prior to its introduction into the glovebox for sample preparation. The NMR tubes were prepared inside the glovebox and then flame-sealed on a vacuum line.

Acknowledgements

A. K. B. thanks the European Union for support through a doctoral grant within the framework of the TMR contract FMRX-CT980174, the Greek State Scholarship Foundation (IKY) for support through a post-doctoral grant, and the Greek General Secretariat of Research and Technology for a grant within the frame of the Competitiveness EPAN 2000–2006, Centers of Excellence #25. We wish to thank Assoc. Prof. G. A. Spyroulias for help with acquisition of the 2D ^1H NMR spectra and Dr. G. A. Tsekouras for help with routines for the treatment of magnetic susceptibility data.

[1] a) G. Christou, D. Gatteschi, D. N. Hendrickson, R. Sessoli, *MRS Bull.* **2000**, *25*, 66–71; b) D. Gatteschi, R. Sessoli, *Angew. Chem.* **2003**, *115*, 278–309; *Angew. Chem. Int. Ed.* **2003**, *42*, 268–297.

[2] M. Cavallini, J. Gomez-Segura, D. Ruiz-Molina, M. Massi, C. Albonetti, C. Rovira, J. Veciana, F. Biscarini, *Angew. Chem.* **2005**, *117*, 910–914; *Angew. Chem. Int. Ed.* **2005**, *44*, 888–892.

[3] a) J. R. Friedman, M. P. Sarachik, J. Tejada, R. Ziolo, *Phys. Rev. Lett.* **1996**, *76*, 3830–3833; b) L. Thomas, F. Lionti, R. Ballou, D. Gatteschi, R. Sessoli, B. Barbara, *Nature* **1996**, *383*, 145–147.

[4] M. N. Leuenberger, D. Loss, *Nature* **2001**, *410*, 789–793.

[5] B. Cage, S. E. Russek, R. Shoemaker, A. J. Barker, C. Stoldt, V. Ramachandaran, N. S. Dalal, *Polyhedron* **2007**, *26*, 2413.

[6] a) R. Sessoli, H.-L. Tsai, A. R. Schake, S. Wang, J. B. Vincent, K. Folting, D. Gatteschi, G. Christou, D. N. Hendrickson, *J. Am. Chem. Soc.* **1993**, *115*, 1804–1816; b) R. Sessoli, D. Gatteschi, A. Caneschi, M. A. Novak, *Nature* **1993**, *365*, 141–143.

[7] D. Li, R. Clérac, S. Parkin, G. Wang, G. T. Yee, S. M. Holmes, *Inorg. Chem.* **2006**, *45,* 5251.

[8] A. M. Ako, I. J. Hewitt, M. Mereacre, R. Clérac, W. Wernsdorfer, C. E. Anson, A. K. Powell, *Angew. Chem.* **2006**, *118*, 5048–5051; *Angew. Chem. Int. Ed. Engl.* **2006**, *45*, 4926–4929.

[9] a) N. Ishikawa, M. Sugita, T. Ishikawa, S. Koshihara, Y. Kaizu, *J. Am. Chem. Soc.* **2003**, *125*, 8694–8695; b) N. Ishikawa, M. Sugita, N. Tanaka, T. Ishikawa, S.-y. Koshihara, Y. Kaizu, *Inorg. Chem.* **2004**, *43*, 5498–5500; c) N. Ishikawa, S. Otsuka, Y. Kaizu, *Angew. Chem.* **2005**, *117*, 741–743; *Angew. Chem. Int. Ed.* **2005**, *44*, 731–733; d) N. Ishikawa, M. Sugita, W. Wernsdorfer, *J. Am. Chem. Soc.* **2005**, *127*, 3650–3651; e) N. Ishikawa, M. Sugita, W. Wernsdorfer, *Angew. Chem.* **2005**, *117*, 2991–2995; *Angew. Chem. Int. Ed.* **2005**, *44*, 2931–2935.

[10] a) S. Karasawa, G. Zhou, H. Morikawa, N. Koga, *J. Am. Chem. Soc.* **2003**, *125*, 13676–13677; b) S. Kanegawa, S. Karasawa, M. Nakano, N. Koga, *Chem. Commun.* **2004**, 1750–1751.

[11] A. J. Tasiopoulos, A. Vinslava, W. Wernsdorfer, K. A. Abboud, G. Christou, *Angew. Chem.* **2004**, *116*, 2169–2173; *Angew. Chem. Int. Ed.* **2004**, *43*, 2117–2121.

[12] A. Tsohos, S. Dionyssopoulou, C. P. Raptopoulou, A. Terzis, E. G. Bakalbassis, S. P. Perlepes, *Angew. Chem.* **1999**, *111*, 1036–1038; *Angew. Chem. Int. Ed.* **1999**, *38*, 983–985.

[13] G. S. Papaefstathiou, S. P. Perlepes, A. Escuer, R. Vicente, M. Font-Bardia, X. Solans, *Angew. Chem.* **2001**, *113*, 908–910; *Angew. Chem. Int. Ed.* **2001**, *40*, 884–886.

[14] G. S. Papaefstathiou, A. Escuer, R. Vicente, M. Font-Bardia, X. Solans, S. P. Perlepes, *Chem. Commun.* **2001**, 2414–2415.

[15] A. K. Boudalis, B. Donnadieu, V. Nastopoulos, J. M. Clemente-Juan, A. Mari, Y. Sanakis, J.-P. Tuchagues, S. P. Perlepes, *Angew. Chem.* **2004**, *116*, 2316–2320; *Angew. Chem. Int. Ed.* **2004**, *43*, 2266–2270.

[16] H. Oshio, N. Hoshino, T. Ito, *J. Am. Chem. Soc.* **2000**, *122*, 12602–12603.

[17] H. Oshio, N. Hoshino, T. Ito, M. Nakano, *J. Am. Chem. Soc.* **2004**, *126*, 8805–8812.

[18] A. K. Boudalis, Y. Sanakis, J. M. Clemente-Juan, A. Mari, J.-P. Tuchagues, *Eur. J. Inorg. Chem.* **2007**, 2409–2415.

[19] A. K. Boudalis, F. Dahan, A. Bousseksou, J.-P. Tuchagues, S. P. Perlepes, *Dalton Trans.* **2003**, 3411–3418.

[20] a) J. M. Clemente-Juan, C. Mackiewicz, M. Verelst, F. Dahan, A. Bousseksou, Y. Sanakis, J.-P. Tuchagues, *Inorg. Chem.* **2002**, *41*, 1478–1491; b) A. K. Boudalis, J. M. Clemente-Juan, F. Dahan, J.-P. Tuchagues, *Inorg. Chem.* **2004**, *43*, 1574–1586.
[21] E. K. Brechin, A. Graham, S. G. Harris, S. Parsons, R. E. P. Winpenny, *J. Chem. Soc. Dalton Trans.* **1997**, 3405–3406, and references therein.
[22] T. Kajiwara, R. Shinagawa, T. Ito, N. Kon, N. Iki, S. Miyano, *Bull. Chem. Soc. Jpn.* **2003**, *76*, 2267–2275.
[23] M. R. Bürgstein, P. W. Roesky, *Angew. Chem.* **2000**, *112*, 559–562; *Angew. Chem. Int. Ed.* **2000**, *39*, 549–551.
[24] M. Addamo, G. Bombieri, E. Foresti, M. D. Grillone, M. Volpe, *Inorg. Chem.* **2004**, *43*, 1603–1605.
[25] K. Manseki, S. Yanagida, *Chem. Commun.* **2007**, 1242–1244.
[26] M. R. Bürgstein, M. T. Gamer, P. W. Roesky, *J. Am. Chem. Soc.* **2004**, *126*, 5213–5218.
[27] X. Hao, Y. Wei, S. Zhang, *Chem. Commun.* **2000**, 2271–2272.
[28] S. Konar, E. Zangrando, M. G. B. Drew, T. Mallah, J. Ribas, N. R. Chaudhuri, *Inorg. Chem.* **2003**, *42*, 5966–5973.
[29] K. L. Taft, C. D. Delfs, G. C. Papaefthymiou, S. Foner, D. Gatteschi, S. J. Lippard, *J. Am. Chem. Soc.* **1994**, *116*, 823–832.
[30] Y. Shapira, M. T. Liu, S. Foner, R. J. Howard, W. H. Armstrong, *Phys. Rev. B* **2001**, *63*, 094422.
[31] C. Dendrinou-Samara, M. Alexiou, C. M. Zaleski, J. W. Kampf, M. L. Kirk, D. P. Kessissoglou, V. L. Pecoraro, *Angew. Chem.* **2003**, *115*, 3893–3896; *Angew. Chem. Int. Ed.* **2003**, *42*, 3763–3766.
[32] a) S. Wang, J.-L. Zuo, H.-C. Zhou, H. J. Choi, Y. Ke, J. R. Long, X.-Z. You, *Angew. Chem.* **2004**, *116*, 6066–6069; *Angew. Chem. Int. Ed.* **2004**, *43*, 5940–5943; b) H. J. Choi, J. J. Sokol, J. R. Long, *Inorg. Chem.* **2004**, *43*, 1606–1608; c) M. Murugesu, J. Raftery, W. Wernsdorfer, G. Christou, E. K. Brechin, *Inorg. Chem.* **2004**, *43*, 4203–4209; d) P. King, W. Wernsdorfer, K. A. Abboud, G. Christou, *Inorg. Chem.* **2004**, *43*, 7315–7323; e) E. M. Rumberger, S. J. Shah, C. C. Beedle, L. N. Zakharov, A. L. Rheingold, D. N. Hendrickson, *Inorg. Chem.* **2005**, *44*, 2742–2752; f) Y. Li, W. Wernsdorfer, R. Clérac, I. J. Hewitt, C. E. Anson, A. K. Powell, *Inorg. Chem.* **2006**, *45*, 2376–2378; g) J. van Slageren, P. Rosa, A. Caneschi, R. Sessoli, H. Casellas, Y. V. Rakitin, L. Cianchi, F. Del Giallo, G. Spina, A. Bino, A.-L. Barra, T. Guidi, S. Carretta, R. Caciuffo, *Phys. Rev. B* **2003**, *74*, 014422.
[33] N. N. Greenwood, T. C. Gibb, *Mössbauer Spectroscopy*, Chapman and Hall, New York, **1971**, pp. 50–53.
[34] J. Chappert, G. Jehanno, F. Varret, *J. Phys. (Paris)* **1977**, *38*, 411–418.
[35] P. Gütlich, R. Link, A. Trautwein, *Mössbauer Spectroscopy and Transition Metal Chemistry*, Springer, Heidelberg, **1978**.
[36] A. Bencini, D. Gatteschi, *EPR of Exchange-Coupled Systems*, Springer, Berlin, **1990**.
[37] A.-L. Barra, P. Debrunner, D. Gatteschi, C. E. Schultz, R. Sessoli, *Europhys. Lett.* **1996**, *35*, 133.
[38] a) A. Caneschi, L. Cianchi, F. Del Giallo, D. Gatteschi, P. Moretti, F. Pieralli, G. Spina, *J. Phys. Condens. Matter* **1999**, *11*, 3395–3403; b) L. Cianchi, F. Del Giallo, G. Spina, W. Reiff, A. Caneschi, *Phys. Rev. B* **2002**, *65*, 064415.
[39] K. L. Taft, A. Caneschi, L. E. Pence, C. D. Delfs, G. C. Papaefthymiou, S. J. Lippard, *J. Am. Chem. Soc.* **1993**, *115*, 11753–11766.
[40] M. P. Hendrich, P. G. Debrunner, *Biophys. J.* **1989**, *56*, 489–506.
[41] F. Hartmann-Boutron, *J. Phys. I* **1995**, *5*, 1281–1300.
[42] A.-L. Barra, L.-C. Brunel, D. Gatteschi, L. Pardi, R. Sessoli, *Acc. Chem. Res.* **1998**, *31*, 460–466.
[43] A. K. Boudalis, N. Lalioti, G. A. Spyroulias, C. P. Raptopoulou, A. Terzis, A. Bousseksou, V. Tangoulis, J.-P. Tuchagues, S. P. Perlepes, *Inorg. Chem.* **2002**, *41*, 6474–6487.
[44] CRYSTALS Issue 10: D. J. Watkin, C. K. Prout, J. R. Carruthers, P. W. Betteridge, Chemical Crystallography Laboratory, Oxford, U.K., CRYSALIS Version 170, Oxford Diffraction, **2002**.
[45] G. M. Sheldrick, SHELXS-97, Program for Crystal Structure Solution, University of Göttingen, Göttingen (Germany), **1990**.
[46] G. M. Sheldrick, SHELXL-97, Program for the refinement of crystal structures from diffraction data, University of Göttingen, Göttingen (Germany), **1997**.
[47] *International Tables for Crystallography, Vol. C*, Kluwer Academic Publishers, Dordrecht, The Netherlands, **1992**.
[48] K. Lagarec, Recoil, Mössbauer Analysis Software for Windows, http://www.physics.uottawa.ca/~recoil.

Received: September 19, 2007
Revised: November 13, 2007
Published online: January 22, 2008

